Journal of Nuclear Materials 404 (2010) 68–76

Contents lists available at ScienceDirect

Journal of Nuclear Materials

journal homepage: www.elsevier.com/locate/jnucmat

# Developing uranium dicarbide–graphite porous materials for the SPES project

L. Biasetto [a,b,*], P. Zanonato [c], S. Carturan [b], P. Di Bernardo [c], P. Colombo [a,d], A. Andrighetto [b], G. Prete [b]

[a] Università di Padova, Dipartimento di Ingegneria Meccanica, Via Marzolo 9, 35131 Padova, Italy
[b] INFN-Laboratori Nazionali di Legnaro, V. le dell'Università 2, 35020 Legnaro (PD), Italy
[c] Università di Padova, Dipartimento di Scienze Chimiche, Via Marzolo 1, 35131 Padova, Italy
[d] Department of Materials Science and Engineering, The Pennsylvania State University, University Park, PA 16802, USA

ARTICLE INFO

*Article history:*
Received 18 November 2009
Accepted 23 June 2010

ABSTRACT

Uranium carbide dispersed in graphite was produced under vacuum by means of carbothermic reduction of different uranium oxides ($UO_2$, $U_3O_8$ and $UO_3$), using graphite as the source of carbon. The thermal process was monitored by mass spectrometry and the gas evolution confirmed the reduction of the $U_3O_8$ and $UO_3$ oxides to $UO_2$ before the carbothermic reaction, that started to occur at $T > 1000$ °C. XRD analysis confirmed the formation of α-$UC_2$ and of a minor amount of UC. The morphology of the produced uranium carbide was not affected by the oxides employed as the source of uranium.



## 1. Introduction

For the next generation of Radioactive Ion Beams (RIB) facilities, robust production targets capable of withstanding irradiation with light ion beams at high power levels for long periods must be developed. These targets should be capable of releasing a broad spectrum of isotopes of a large number of elements, with short-lifetime (less than 100 ms).

As tested in the past at ISOLDE [1] and recently studied at HRIBF [2], uranium carbide (namely $UC_x$, with $1 \leqslant x \leqslant 2$) dispersed in excess graphite is the ideal candidate as target material for the production of RIB. Even though the release of nuclear reactions products has been extensively studied for RIB production [2,3] the reasons for the good release properties of this material are not yet fully understood.

Since the process of isotopes release consists of diffusion within the grain and effusion towards the ionization source, the composition, the density and the operating temperature of the material constituting the target are important parameters to be considered.

In order to achieve the best performance, the target material should respond to stringent requirements, such as:

(1) to have large cross section and diffusion coefficient;
(2) to work at the highest possible operating temperature, defined as the temperature at which its vapor pressure begins to affect the ionization efficiency of the ion source used in the exotic ions generation;
(3) to possess high emissivity and high thermal conductivity, responsible for heat dissipation during the target bombardment: a good heat dissipation of the target prevents its overheating and mechanical stresses; and
(4) to exhibit low density and high permeability to the effusion of the produced isotopic species. The presence of open porosity favors both diffusion and permeability [4].

For all the above mentioned reasons, among the possible choices for the materials constituting the SPES target, low density, carbon dispersed metal carbides ($MC_x$) have been chosen as target material. The SPES project, now under development at LNL-INFN [5,6], is an Isotope Separation On Line (ISOL) facility designed for the production of intense neutron-rich exotic species ($A = 80$–160). The SPES project is the main nuclear physics project in Italy for the next years, and is expected to run the first exotic beam in 2014. The target, the core of the ISOL facility, consists of seven separate thin (1 mm thickness) disks, directly impinged by a 40 MeV (200 μA) proton beam. The target design allows for nuclear fission reactions with high fission rate. The operating temperature should be as high as 2000 °C to enable high diffusion rate. Thermo-mechanical calculations [7] have shown that the SPES target, with its innovative production core, can stand the 8 kW impinging proton beam which produce about $10^{13}$ fissions/s in the target. The short-lifetime neutron-rich exotic isotopes, produced by means of nuclear fission reactions occurring in the disks, must diffuse and eventually effuse to the ionization chamber in the shortest time to avoid their condensation on the cold target regions and their decay before reaching the ionization chamber.

It is then clear that the target composition and morphology play a key role in the design of the primary ion source for the facility.

As reported in the literature [8–11] uranium carbide exists in three stoichiometric phases: UC, $U_2C_3$ and $UC_2$. Uranium

* Corresponding author at: INFN-Laboratori Nazionali di Legnaro, V. le dell'Università 2, 35020 Legnaro (PD), Italy.
*E-mail address:* lisa.biasetto@lnl.infn.it (L. Biasetto).

0022-3115/$ - see front matter © 2010 Elsevier B.V. All rights reserved.
doi:10.1016/j.jnucmat.2010.06.032

monocarbide is face-centered cubic, and it is the most stable phase from room temperature up to 2526 °C. Uranium sesquicarbide is cubic body centered and is metastable at low temperature [10]. It starts to become stable at approximately 900 °C up to 1816 °C, where it decomposes to form UC and $UC_2$. Uranium dicarbide is stable at high temperatures, it forms above 1470 °C, and it probably melts at 2427 °C. Two polymorphs of $UC_2$ exist: the high temperature cubic form and the low temperature tetragonal form, with the transformation occurring at approximately 1771 °C. The carbides of uranium, in particular UC and $UC_2$, are difficult to prepare free from oxygen and nitrogen contamination [12–14], especially when produced by carbothermic reduction of the precursor oxide. Also, a few weight percentage of oxygen or nitrogen in the sample constitute a substantial atomic percentage, forming a solid solution in the monocarbide or dicarbide structure. These impurities within the uranium carbide structure deform the unit cell geometry [8,9,13] and, in the case of uranium dicarbide, might have also a stabilizing effect on this phase at room temperature [15].

Uranium carbides can be produced by arc melting of metallic uranium with carbon or by direct solid state reaction of the elements at high pressure, according to Eq. (1) [16],

$$xU + zC \rightarrow U_xC_z \quad (1)$$

with $z/x = 1, 1.5, 2$.

Another method consists in the carbothermic reaction of the metal oxide with carbon (graphite powder or other carbon precursors), Eq. (2):

$$U_xO_y + (z+y)C \rightarrow U_xC_z + yCO \quad (2)$$

In addition uranium carbide can be produced by the reaction of the metallic uranium with $CH_4$ following equation:

$$xU + zCH_4 \rightarrow U_xC_z + 2zH_2 \quad (3)$$

The reaction temperature decreases from Eqs. (1)–(3) and it is strictly dependent on the processing conditions.

The $UC_x$ for the SPES target is produced under vacuum by the carbothermic reaction (2).

The reason for the use of this processing condition lies on:

(1) the lower temperature needed by the carbothermic reaction, compared to the same process carried out under inert atmosphere; and
(2) the formation of pores, resulting from the CO released during the carbothermic reduction that occurs at $T > 1000$ °C.

The sinterization process, which takes place at higher temperatures than the carbothermic reduction, can cause pores of small dimension to collapse if sinterization is not appropriately controlled. This shortcoming makes it very difficult to properly control the amount and type of porosity generated by the thermal treatment.

More porosity can be introduced in the target material at lower temperatures by several methods:

(1) the use of suitable precursors for metal oxide. For example, carbonates, mono-or di-carboxylates that decompose to oxides releasing CO and/or $CO_2$ [17];
(2) the use of organic fillers that decompose totally or produce carbon releasing water, CO, $CO_2$ and other gaseous species; and
(3) the addition to the properly modified reaction mixture of a polymeric expanding agent.

Previous attempts for the production of porous uranium carbide used the carbothermic reduction of uranium oxide or an interconnected matrix (fibrous SiC, graphite cloth or reticulated vitreous carbon foam) as a support for a thick film of a suitable uranium carbide [18].

Recently, the usage of lanthanum dicarbide ($LaC_2$) was suggested as a substitute of uranium compounds for preliminary bench tests on the production and characterization of highly porous carbides [17,19–21]. In [17,19,20], the development of lanthanum carbide possessing a controlled amount of porosity, with dimensions ranging from few nanometers to some microns was achieved by using oxalate instead of oxides as precursors for lanthanum, and using carbon nanotubes as the source of carbon.

Even though uranium carbide has been extensively used in the RIB facilities worldwide, only limited information is available in the literature concerning the composition and morphology of the targets. For instance, there has been some confusion about whether target material is UC or $UC_2$ [2]. Since the material composition and morphology are strictly dependent on processing conditions, and several methods have been so far employed for the production of the uranium carbide targets for RIB production, some uncertainties exist on the actual properties of the final material.

However, the research in the field of the uranium–oxygen–carbon system is currently very lively mainly because of its growing importance for the prediction of the behavior of Tri-ISOtropic (TRISO) fuel particle in the generation IV nuclear reactors [22]. This interest is driven by the need for predicting the fuel particle behavior in case of nominal or accidental conditions.

In this work, the first systematic study on the effects of changes of the starting mixtures ($UO_2$/C, $U_3O_8$/C, $UO_3$/C) on the final material characteristics (composition, emissivity, degree of sinterization, porosity amount and pore size, and interconnectivity of the pores) is presented.

## 2. Experimental

Porous $UC_x$ based composites in graphite were prepared by means of thermal treatment of $UO_2$, $U_3O_8$, $UO_3$ and graphite mixtures following Eq. (4), keeping the $x/n$ ratio equal to 1/4.

$$U_xO_y + (z+y+n)C \rightarrow U_xC_z + nC + yCO \quad (4)$$

The $UO_2$ and $U_3O_8$ were purchased from CERAC Inc. (Milwaukee, WI, USA) powders size < 300 μm, graphite (powders size < 45 μm) from Sigma–Aldrich and all used as received.

$UO_3$ was prepared from uranyl nitrate hexahydrate (Sigma–Aldrich), according to the method proposed by Allen [23]. A batch of about 10 g of the compound was gradually heated up to 350 °C in a crucible and left to stand overnight. The resulting dark red–orange compound was finely ground in an agate mortar.

Powders ($U_xO_y$ and graphite) were manually ground and mixed in an agate mortar, inside a glove-box ($O_2$ and $H_2O$ ppm < 1), the weight percentages of the powders complying with the stochiometry of Eq. (4); 2 wt.% of phenolic resin was added as a binder. After mixing, the powders were placed in a 13 mm diameter mold and were uniaxially cold pressed at 750 MPa. The green samples possessed a nominal diameter of 13 mm, 1 mm thickness and approximately 350 mg weight. In Table 1 is reported an overview of the prepared samples.

The thermal treatment was performed under high vacuum ($10^{-4}$–$10^{-5}$ Pa) in a graphite crucible using the experimental set-

**Table 1**
Overview of the prepared samples.

| Sample | $UO_2$ (wt.%) | $U_3O_8$ (wt.%) | $UO_3$ (wt.%) | $C_{graphite}$ (wt.%) |
|---|---|---|---|---|
| $UO_2C$ | 79.2 | – | – | 20.8 |
| $U_3O_8C$ | – | 77.8 | – | 22.2 |
| $UO_3C$ | – | – | 77.4 | 22.6 |

up described in [24]. The heating schedule was designed in order to:

(1) promote the carbothermic reaction (2 °C/min up to 1250 °C, 24 h at 1250 °C); and
(2) sinter the carburized powders (2 °C/min up to 1600 °C, 4 h at 1600 °C).

A slow cooling was performed at a rate of 2 °C/min up to room temperature.

The heating process was monitored by means of a penning trap which measured the pressure inside the chamber (in the $10^{-1}$–$10^{-5}$ Pa pressure range) and by a Quadrupole Mass Spectrometer (QMG 220 Pfeiffer Vacuum Italy SpA, Rho-MI Italy) up to 300 amu/e. Both the starting powders ($UO_2$ $U_3O_8$ and $UO_3$) and the final samples were analyzed by X-ray Diffractometry using Cu-Kα radiation (Philps PW 1710, XRD). During the analysis, the powders were protected from the environment by a PEEK® film (VICTREX- UK, 25 μm thickness). After carburization and sinterization, the samples were stored in a glove-box ($O_2$ and $H_2O$ ppm < 1). Samples were weighted and their dimensions were recorded. The bulk density ($\rho_{bulk}$) was measured by the weight over volume ratio. The theoretical density ($\rho_{th}$) was calculated as the weighted average, taking into account the values of 11.2 g/cm$^3$ and 1.9 g/cm$^3$ for the theoretical density of $UC_2$ and graphite, respectively.

The apparent density of the samples, $\rho_{ap}$, was measured by He Pycnometry (AccuPyc1330, Micromeritics Italia), in order to calculate the amount of open ($P_{open}$), and closed ($P_{closed}$), porosity according to following equations:

$$P_{tot} = 1 - \frac{\rho_{bulk}}{\rho_{th}} \quad (5)$$

$$P_{open} = 1 - \frac{\rho_{ap}}{\rho_{th}} \quad (6)$$

$$P_{tot} = P_{open} + P_{closed} \quad (7)$$

The morphology and composition of the samples were studied by Scanning Electron Microscopy (Philips XL-30, SEM) equipped with EDS probe (Energy Dispersive Spectrometer). The SEM images and EDS spectra were taken with primary electron beam energy of 10 keV. When analyzing the composition of the composites, only larger particles were analyzed with high magnification in order to avoid interference from the surrounding matrix.

A preliminary study of the $UC_x$ dispersed in graphite reactivity towards the environment was carried out by analyzing by SEM–EDS samples that were exposed for 48 h to ambient air at 20 °C, with a relative humidity of 87%. The emissivity of the samples was measured using a double frequency infrared pyrometer (Modline5, IRCON, USA, working wavelength bands 0.85–1.05 μm and 1–1.10 μm, calibrated according to the Quality System ISO 9001:2000) as reported in [24]. The pyrometer was settled normal to the sample surface with radiation passing through a borosilicate glass window (Kodial view port, Torr Scientific Ltd., East Sussex-UK) almost completely transparent to infrared radiation (transmission up to 95%). In the measurements performed in this work the gray body hypothesis was assumed. The emissivity values were monitored during the heat treatments of the samples that were repeated at least three times. The calculated standard deviation from the average values was 1%.

## 3. Results and discussion

Even though the uranium–oxygen system is a key system in the nuclear materials field, and many thermodynamic data can be found in the literature, still some uncertainties are present about the identification of the range of stability of the different uranium oxides. Because of the numerous oxidation states of uranium, several oxides exist such as $U_4O_9$, $U_3O_8$ and $UO_3$. Uranium dioxide ($UO_2$) represents the compound with the widest stability range at high temperature. It can often be found as a hypo- or hyper-stoichiometric compound, generally labeled as $UO_{2\pm x}$ (with $-0.4 < x < 0.3$) [25–27].

The choice of using $UO_2$, $U_3O_8$ and $UO_3$ for the present study was driven by the possibility of introducing a different amount of porosity in the final material as effect of the different reaction pathways with carbon of the selected uranium oxides.

The results of the XRD analysis performed on the starting oxide powders, used as uranium source for the carbothermic reaction, are reported in Fig. 1. As can be observed, the commercial $UO_2$ and the synthesized $UO_3$ gave XRD spectra corresponding to the expected cubic structures of $UO_2$ and $UO_3$. On the other hand, XRD spectrum of commercial $U_3O_8$ indicates the probable presence of cubic $UO_3$ together with the monoclinic $U_3O_8$ phase. Because of the overlapping of the spectra of the two species, it is however not easy to estimate the relative amount of the higher oxidation state oxide in the mixture.

In order to achieve a homogeneous dispersion of graphite and uranium oxide the mixing and grinding of the reagent powders had to be conducted very carefully. This is a key point in the preparation of the samples, since the reaction between the $U_xO_y$ and carbon is controlled by the diffusion of carbon and oxygen [28], so that a good contact between the reactants is necessary for the reaction to proceed satisfactorily.

Analysis of the evolution of the gaseous species upon carburization and sinterization is reported in Fig. 2, in which the total pressure inside the chamber is reported vs. temperature of the treatment. As it can be observed, for all the samples a wide out-gassing starts at ~100 °C and evolves up to the final sinterization temperature of 1600 °C.

Thermal treatments above the latter temperature are not reported in this preliminary study that concerns the evolution of porosity in the sample.

As already discussed in the experimental part, the thermal treatment was designed in order to promote the carburization of the oxides, which was expected to occur at $T > 1000$ °C. However, in the thermal treatment the amount of gas evolved before carburization ($T < 1000$ °C) is abundant for all the three samples, in particular for $UO_3$ and $U_3O_8$ containing samples.

This low-temperature out-gassing can be attributed to at least three different causes:

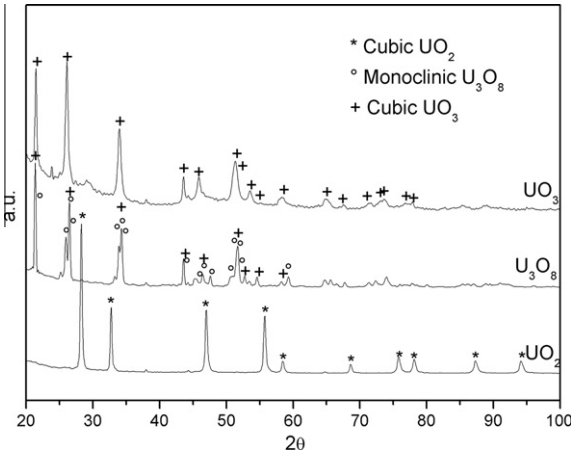


**Fig. 1.** X-ray Diffraction patterns of the starting oxide powders ($UO_2$, $U_3O_8$ and $UO_3$).

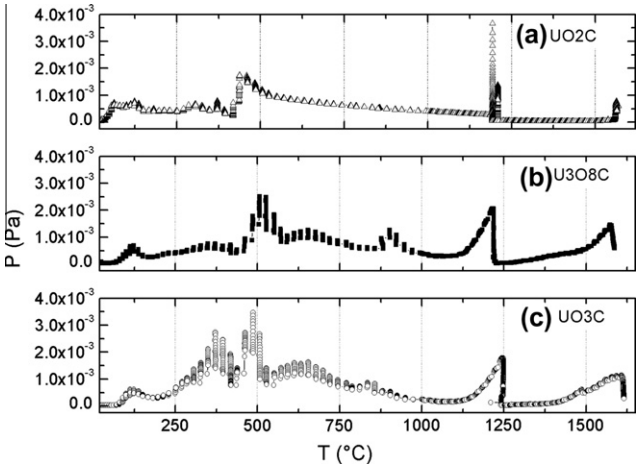


**Fig. 2.** Pressure evolution upon carburization and sinterization of the $UO_2C$ (a), $U_3O_8C$ (b) and $UO_3C$ (c) samples.

- the elimination of adsorbed water from the powders of oxides and graphite;
- the decomposition of the phenolic resin used as binder, which thermal gravimetric analysis indicates to occur in the 350 °C–800 °C temperature range; and
- the reduction of $UO_3$ and $U_3O_8$ to $UO_2$, with release of oxygen mono or dicarbide.

For $T > 1000$ °C, two main peaks can be observed and they can be both attributed to the carbothermic reduction transforming oxides into carbides.

These considerations were confirmed by analysis of the gas atmosphere in the vacuum furnace achieved by mass spectrometry. It was observed in fact that two species, water (at 18 amu/e) and carbon monoxide (at 28 amu/e) were detected in abundance during the thermal treatment. Moreover, the presence of carbon dioxide (at 44 amu/e), even if to a lesser extent, was found to be relevant. Hence, to monitor the progress of the reactions in the vacuum furnace, the evolution of the three species was followed, recording the ionization current at 18, 28 and 44 amu/e during the thermal process.

In Fig. 3, the ionization current at 18 amu/e is plotted against temperature. The shape of the curve is similar for all the three samples, and can be attributed mainly to $H_2O$ coming from the decomposition of the phenolic resin [17,19,20] and to the little water present in the set-up and adsorbed in the reagent mixture.

In Fig. 4, the ionization current at 44 amu/e is plotted against temperature. Only the samples containing $UO_3$ and $U_3O_8$ showed evolution of $CO_2$, while the sample containing $UO_2$ did not.

The $UO_3C$ sample revealed the presence of two peaks centered at approximately 350 °C and 450 °C, while the $U_3O_8C$ sample had only one peak at approximately 500 °C. These data are consistent with the literature that describes the carboreduction of $UO_3$ to $UO_2$ via $U_3O_8$ at similar temperatures [29]. The reduction mechanism, at atmospheric pressure and under helium flow, has been recently described in detail by Poncet and co-workers [30].

A two steps reduction involving carbon, as reducing agent, and $CO_2$, as evolving gas, is postulated:

First, at 450 °C, $UO_3$ is reduced to $U_3O_8$,

$$6UO_3 + C \rightarrow 2U_3O_8 + CO_2 \quad (8)$$

Successively, at 590 °C, $U_3O_8$ forms $UO_2$,

$$U_3O_8 + C \rightarrow 3UO_2 + CO_2 \quad (9)$$

The two peaks observed in Fig. 4 for the $UO_3C$ sample at 350 °C and 450 °C can therefore be attributed to the $CO_2$ evolution corresponding to the reduction of $UO_3$ to $U_3O_8$ (Eq. (8)) and of $U_3O_8$ to $UO_2$ (Eq. (9)) respectively. Accordingly, the $U_3O_8C$ sample shows only one peak at 500 °C, corresponding to the reduction of $U_3O_8$ to $UO_2$, with $CO_2$ evolution (Eq. (9)). The lower temperatures observed in our case for reactions (8) and (9) as compared to the results of Poncet are in good agreement with those of Mukerjee [34], whose reaction condition are similar to those used in the present work and can be ascribed to the influence of dynamic high vacuum in the reaction chamber, that favors the reactions. The small release of $CO_2$ by the $U_3O_8C$ sample at $200 < T < 400$ °C can be explained by the presence of a relatively small amount of $UO_3$, as the XRD spectrum of commercial $U_3O_8$ indicated. The $CO_2$ evolution was complete for $T > 700$ °C, and this suggests that the transformation of $UO_3$ and $U_3O_8$ to $UO_2$ is complete before carburization.

In Fig. 5 is reported the CO evolution (at 28 amu/e) at increasing temperature, for the three samples.

The origin of the moderate evolution of CO at $T < 1000$ °C for the $UO_3C$, $U_3O_8C$ and $UO_2C$ samples is not yet fully understood. The presence of hyper-stoichiometric oxide, namely $UO_{2+x}$, in the $UO_2C$ sample can partially explain the production of carbon

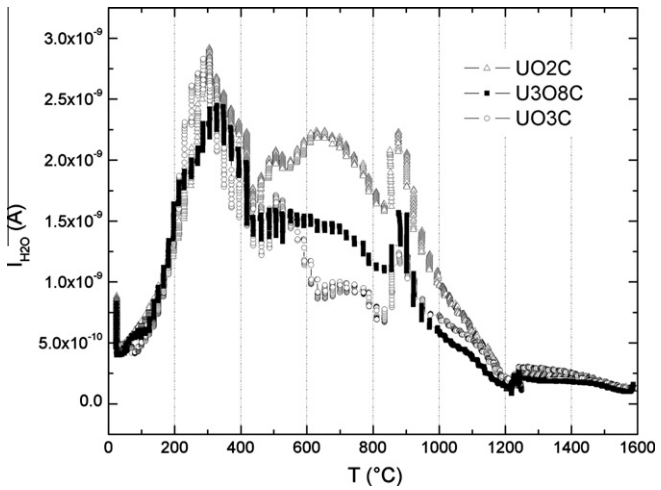


**Fig. 3.** $H_2O$ evolution (18 amu/e) upon carburization and sinterization of the $UO_2C$, $U_3O_8C$ and $UO_3C$ samples.

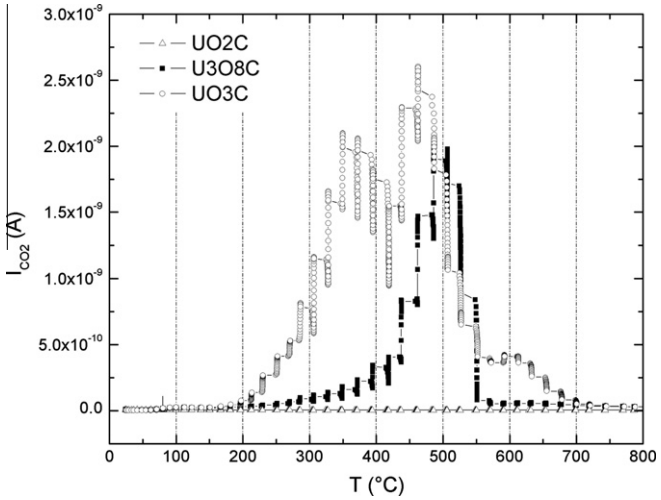


**Fig. 4.** $CO_2$ evolution (44 amu/e) vs. temperature upon carburization and sinterization of the $UO_2C$, $U_3O_8C$ and $UO_3C$ samples.

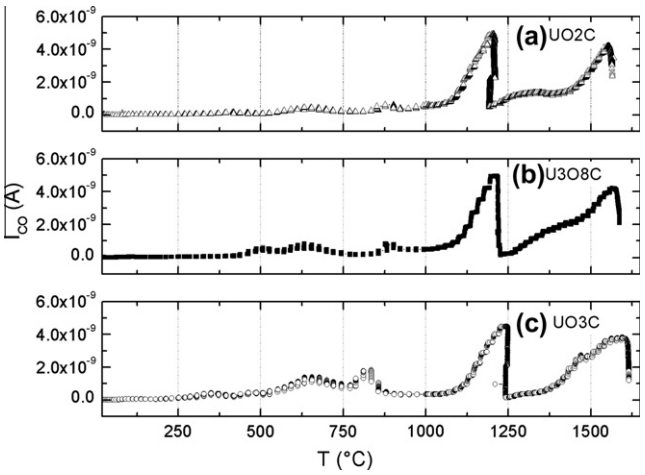


**Fig. 5.** CO evolution (28 amu/e) vs. temperature upon carburization and sinterization of the $UO_2C$ (a), $U_3O_8C$ (b) and $UO_3C$ (c) samples.

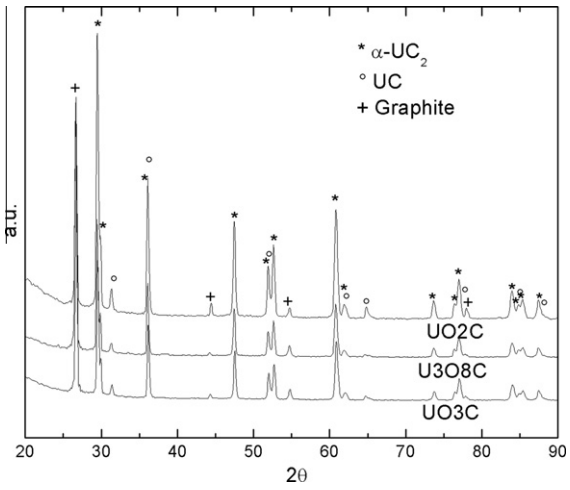


**Fig. 6.** XRD patterns for the carburized samples.

monoxide at these temperatures, as the consequence of the reduction of uranium dioxide to hypo-stoichiometric $UO_{2-x}$ [31–33].

As far as $UO_3C$ and $U_3O_8C$ are considered, in apparent disagreement with the experimental results of Poncet et al. [30] and Mukerjee [34], who proved that only $CO_2$ evolves during the carbothermic reduction of $UO_3$, we observed a significant release of CO, in the case of sample $UO_3C$, at 800 °C, that is about 100 °C above the end of the carbon dioxide production. A peak of lower intensity at 900 °C is also present in the $U_3O_8C$ and $UO_2C$ samples.

However, as pointed out by Poncet et al. [35] at temperatures higher than 800 °C it is possible to form CO gas according to the Boudouard equilibrium:

$$CO_2 + C \rightarrow 2CO \quad (10)$$

Hence, the remarkable CO evolution at temperatures as high as 800 °C in the $UO_3C$ sample can be ascribed to the reaction of residual $CO_2$, released during reactions (8) and (9), adsorbed on the surface of graphite grains. Moreover, for all the three samples $UO_2C$, $UO_3C$ and $U_3O_8C$, CO release is expected to derive from thermal degradation of the phenol-based resin, used as a binder.

For $T > 1000$ °C, the CO evolution can be attributed to the carbothermic reduction of $UO_2$ and the consequent formation of uranium carbides. The two peaks at 1200 °C and 1600 °C corresponds to the plateaus of the heating ramp. The shape of the pattern describing the evolution of CO in the reaction between the uranium dioxide and graphite in the 1100–1600 °C temperature range can be attributed to the presence of a gradient in temperature within the samples (with temperature decreasing from the bottom to the top of the samples, as they were heated by contact with a graphite electrode on which they were placed).

The XRD analysis of the resulting materials, reported in Fig. 6, revealed the presence of tetragonal $UC_2$ ($\alpha UC_2$), graphite and a minor amount of cubic face centered UC. Literature data [36] confirm that UC can be produced by the carbothermic reaction of uranium oxide with graphite at lower temperatures than uranium dicarbide, in the presence of a $C/UO_2$ molar ratio of 3.0 [37] following the reaction below:

$$UO_2 + 3C \rightarrow UC + 2CO \quad (11)$$

When produced by this route, the resulting uranium monocarbide invariably contains 950–1100 ppm of oxygen, in the form of compound ($UO_2$) or solid solution ($UC_{1-x}O_x$) [13].

In this study, the presence of uranium monocarbide and carbon (as graphite), besides tetragonal uranium dicarbide, may be attributed to the precipitation of carbon from the uranium dicarbide at some intermediate temperature during the slow cooling from the sinterization temperature [8] (the cooling rate was 2 °C/min). In [8], samples that were quenched from high temperature, presented carbon in solid solution with uranium dicarbide, and consequently decreased lattice constants (i.e. $a = 3.504$ A, $c = 5.951$ A). The $\alpha UC_2$ synthesized in this work, presented a good fitting with X-rays patterns for a tetragonal cell of $a = 3.522$ Å and $c = 5.988$ Å and, as reported in [9], to the elongated fluorite structure.

From a thermodynamic point of view [8,38,10,39] (Eq. (4)), the formation of $U_2C_3$ should theoretically be considered at the final atomic ratio C/U = 4, even though Benz [10] suggested a dotted line for $U_2C_3$ at $T < 900$ °C in the U/C phase diagram, which takes into account the supposed metastability of the sesquicarbide at low temperature, in agreement with other observations. As reported in [40], uranium sesquicarbide is very difficult to obtain. It can be produced from $UC–UC_2$ mixture by cooling from 1250 to 1800 °C and the application of a mechanical stress [40].

The presence of oxygen contamination in the uranium carbide produced in this work could not be detected by the standard chemical analysis techniques available in our laboratory. Accordingly, XRD measurements on $UC_x$ based composite in graphite did not show formation of oxygen compounds; neither as uranium oxycarbide nor as uranium oxide (see Fig. 6). This indicates that the oxygen contamination in the samples, is less than the limit of resolution of the instrument (<4 wt.%).

In order to describe the process of formation of uranium carbide by carbothermic reaction, the reaction kinetics of the system $UO_2$–C should also be taken into account. Stinton [41] and Mukerjee and co-workers [42] studied in great detail the carbothermic reaction kinetics of the system $UO_2$ + C, under both vacuum and flowing argon in the 1250–1500 °C temperature range. For experiments conducted in vacuum, Mukerjee deduced a reaction mechanism governed by reagent-product interface reactions, where the limiting step is the $UO_2/UC_2$ interface reaction, whereas in the case of flowing argon the rate limiting step is the diffusion of CO through the newly formed carbide layer. In both the synthetic routes, Mukerjee observed that, depending on the C/U molar ratio (varying between 3.0 and 4.0), the product was UC, a mixture of UC + $UC_2$ or $UC_2$. $U_2C_3$ was not observed as a product, not even as an intermediate product.

In the case of carbothermic reduction under vacuum, Mukerjee assessed that for loose powder mixtures the escape of CO through the carbide layer is fast and does not affect the reaction kinetics. However, in case of tight compacts of $UO_2$ + C the reaction is governed by CO diffusion mechanisms, as pointed out by Suzuki [43]

and quoted by Mukerjee [42]. Hence, in the experimental conditions used for the present work, where uranium oxide powders and graphite were compacted under high pressure, it can be deduced that a diffusion controlled reaction pathway is attained, thereby enabling the occurrence of the following reaction (Eq. (12)) at the final stages of the synthesis

$$3UC_2(s) + UO_2(s) \rightarrow 4UC(s) + 2CO(g) \quad (12)$$

Hence, a thin layer of UC between $UC_2$ and the residual unreacted $UO_2$ particle core can be produced, as a result of the CO diffusion slowed down by the thick layer of $UC_2$.

A confirmation of the proposed reaction sequence, leading to the formation of a minor amount of UC besides the main product $UC_2$, can be found in the work of Gossé and co-workers [31], who recently reported the effects of kinetic limitations concerning the interaction between $UO_2$ and C. Their high temperature mass spectrometry experiments performed on $UO_2$ + C pellets (in stoichiometric ratio) confirmed the strong interaction between these two compounds at $T > 700$ °C. When $UO_{2+x}$ reached an almost stoichiometric composition, a carbide phase began to form and a three phase domain was attained, where $UO_2$, C and UC coexist.

In Table 2, the measured and calculated weight losses after carburization and sinterization are reported. As it can be observed, the experimental weight loss values increase, in agreement with the calculated ones, from $UO_2C$ to $UO_3C$ samples, in good agreement with the reduction of $UO_3$ and $U_3O_8$ reported above (Eqs. (2) and (3)). The measured bulk density values do not significantly vary from $UO_2C$ to $UO_3C$. On the other hand, the apparent density measured using a He-pycnometer reveals a trend from $UO_2C$ to $UO_3C$, increasing with the oxidation number of the oxide. Consequently, the total porosity (calculated by Eq. (5), true density equal to 10.41 g/cm$^3$) ranges from 62.5 vol.% for the $UO_2C$ sample to 64.4% for the $U_3O_8C$ sample, the open and closed porosity are approximately constant for the three oxides, with a slight increase of closed porosity passing from $UO_2C$ (6%) to $UO_3C$ (8%). The volume shrinkage strongly varied with each processing and sample, so that no clear trend could be identified.

From a morphological point of view, the three samples did not show any significant difference among them. SEM–EDS analyses, performed on the surface of each sample at different magnifications, are reported in Fig. 7. White–gray and black–gray islands of large dimensions (>10 μm) with homogeneous distribution are clearly visible at low magnifications. These white–gray and black–gray islands can certainly be attributed to uranium carbide and graphite respectively, as confirmed by EDS analysis (see also Fig. 8). Macropores of irregular shape and some microns in size can be detected at both low and high magnification. The shape and dimensions of these pores is quite similar to that of the graphite powders used as source of carbon for the carbothermic reduction of the precursor oxides. At higher magnification, macropores of smaller dimensions are also visible, and they can be attributed to the incomplete sinterization of the uranium carbide grains.

As for the air stability of the produced uranium carbide based samples, a simple experiment was conducted, by exposing the sample $UO_3C$, after SEM–EDS analysis, to ambient air (20 °C, R.H. 87%) for 48 h and again analyzing the sample with SEM–EDS. Previous literature data [44] showed that hydrolysis of uranium dicarbide produced complex mixtures of gaseous hydrocarbons, hydrogen, and a hydrous uranium oxide.

Moreover, as reported in [43], the variation of the reaction temperature between 25 and 99 °C produced no detectable effect on the composition of the gas in the hydrolysis of the dicarbide. However, the hydrolysis rate increased markedly with increasing temperature and the time required for complete reaction of the uranium dicarbide (3–4 g) varied from 3.5 days at 25 °C to about 3 h at 99 °C.

Whereas the hydrolysis mechanism, as for both reaction products and kinetics, was extensively studied for several uranium carbides and mixtures thereof, the hydrolysis in moist air of uranium dicarbides was studied to a lesser extent. In the work of Engle and co-workers [45], the exposure to moist air of thorium–uranium dicarbides was studied as related to reaction rate as a function of surface area of the reacting particle and temperature. The reaction rate for $UC_2$ exposed to moist air at 30 °C was much smaller as compared to $ThC_2$, and the weight gain (%) was less than 0.2% after 18 h of reaction.

In Fig. 8, the EDS spectra collected from a spot on a white grain of carbide of the sample $UO_3C$ before and after exposure are reported. The spectra are normalized on the intensity of uranium peak (M line), in order to better highlight the change in carbon and oxygen signals. Both the depletion in carbon content and enrichment in oxygen are clearly observed, though significant changes in grains morphology are not evidenced from SEM images (Fig. 8). The sample surface composition, as derived from EDS analyses of several carbide grains of the sample before and after exposure, is reported in Table 3. The presence of surface oxygen on the unexposed sample has been already observed for lanthanum carbide based samples and it can be attributed to the following reasons [13]:

- Incomplete milling and mixing of graphite and $U_xO_y$ powders.
- Limitations to forced evacuation of CO from closed pores formed by sinterization during heating, and to the evacuating capability of experimental equipment.
- Adsorption of oxygen during samples removal from vacuum furnace and contamination from impurities contained in the inert gas in the vessels.

The trend in both carbon and oxygen amounts is again evidenced, but the measured values are affected by a remarkable experimental error, thereby preventing a quantitative determination of the hydrolysis reaction extent and a comparison with previously reported literature data. A more thorough investigation on the hydrolysis rate, relying on XRD analyses and gravimetric measurements as a function of the exposure time, is currently in progress.

The emissivity measurements, performed upon carburization and sinterization (Fig. 9), revealed a similar trend for $UO_2C$, $U_3O_8C$ and $UO_3C$ samples. It is well known that emissivity is affected by multiple factors, such as temperature, wavelength, direction, atmosphere conditions, surface roughness, oxidation level, material grain size and porosity. Previous studies were performed to measure emissivity of uranium carbides [46–48]. In particularly, for nearly stochiometric $UC_2$ specimens (99.5% of theoretical density) the measurement revealed constant values of emissivity of

**Table 2**
Calculated and measured weight loss, bulk ($\rho_b$) and apparent ($\rho_{ap}$) density, total, open and closed porosity.

| Sample | $\Delta wt_{calculated}$ % | $\Delta wt_{measured}$ % | $\rho_b$ (g/cm$^3$) | $\rho_{ap}$ (g/cm$^3$) | $p_{tot}$ (vol.%) | $p_{open}$ (vol.%) | $P_{closed}$ (vol.%) |
|---|---|---|---|---|---|---|---|
| $UO_2C$ | 16.9 | 17.3 ± 0.8 | 3.9 ± 0.1 | 9.0 ± 0.1 | 62.5 ± 1 | 56.6 ± 0.6 | 5.9 ± 0.4 |
| $U_3O_8C$ | 20.2 | 20.2 ± 0.7 | 3.7 ± 0.2 | 8.7 ± 0.2 | 64.4 ± 1.9 | 57.4 ± 1.4 | 7 ± 0.5 |
| $UO_3C$ | 21 | 22.6 ± 0.9 | 3.8 ± 0.1 | 6.8 ± 0.1 | 63.5 ± 1 | 55.5 ± 1.5 | 8 ± 0.5 |

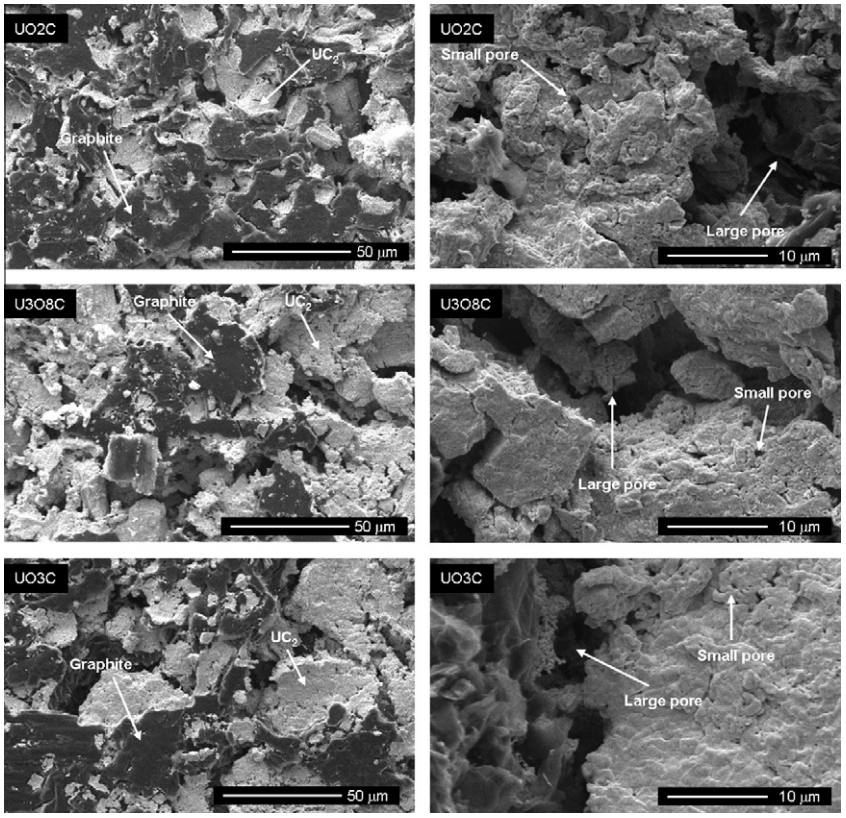


**Fig. 7.** SEM analysis of $UO_2C$, $U_3O_8C$ and $UO_3C$ samples.

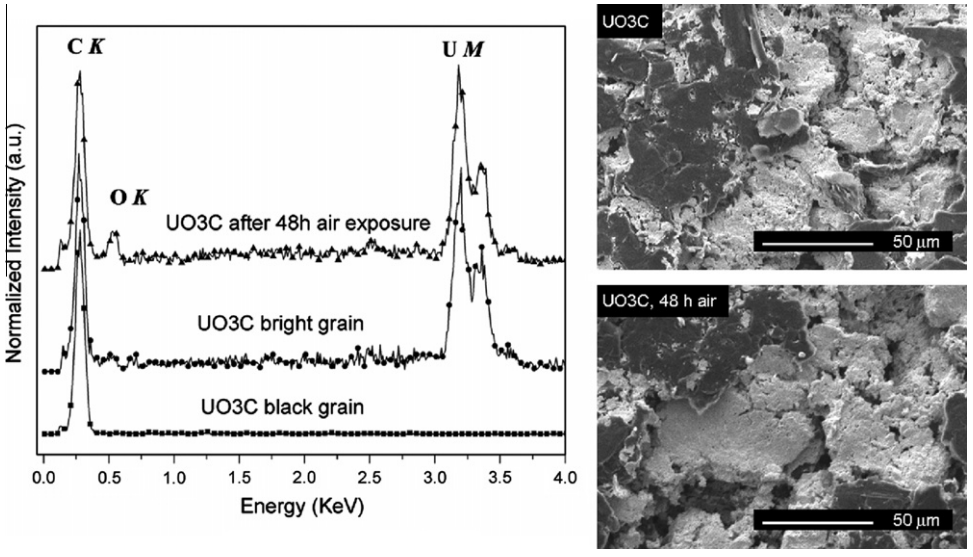


**Fig. 8.** Effect of air exposure on $UO_3C$ sample, EDS left and SEM at the same magnification before and after air exposure, right.

**Table 3**
EDS compositional analyses of the white carbide grains of the sample $UO_3C$ before and after exposure to moist air. Each value represents the average of at least six measurements, the error was calculated as standard deviation of experimental data.

| Sample | C (wt.%) | O (wt.%) | U (wt.%) | C (at.%) | O (at.%) | U (at.%) |
|---|---|---|---|---|---|---|
| $UO_3C$ | 13.6 ± 2.8 | 2.8 ± 0.7 | 83.7 ± 2.8 | 68.1 ± 5.3 | 10.2 ± 2.4 | 21.7 ± 4.0 |
| $UO_3C$ exposed | 12.4 ± 1.7 | 7.0 ± 1.7 | 80.6 ± 3.1 | 56.9 ± 2.9 | 24.1 ± 3.6 | 19.0 ± 3.0 |

0.495 and of 0.55 for wavelength ($\lambda$) of 2.3 μm and 0.65 μm in the 1800–2060 °C temperature range. In the case of the 1040–1740 °C temperature range a linear dependence of emissivity with temperature was observed (intercept 0.4067 at $T$ = 1040 °C and slope

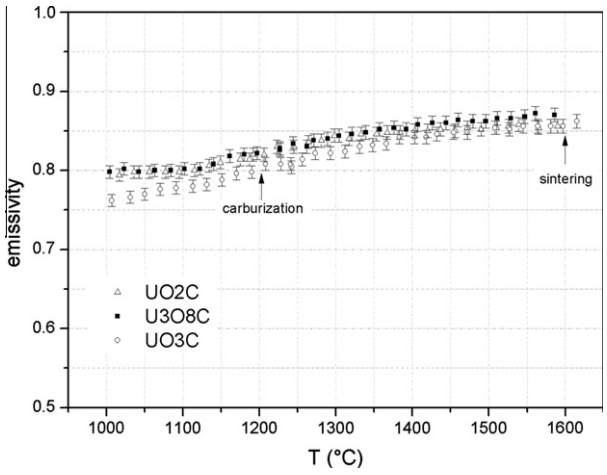


**Fig. 9.** Emissivity measurements of the $UO_2C$, $U_3O_8C$ and $UO_3C$ samples upon carburization and sinterization.

$4.067 \times 10^{-5}$ for $\lambda = 0.65$ μm; intercept 0.423, slope $1.55 \times 10^{-5}$ for $\lambda = 2.3$ μm) that is the case of interest for our experiment; our measurements were indeed run during the carbothermic reduction and sinterization of the produced carbides.

The data reported in Fig. 9 shows that emissivity increased at increasing temperatures. At 1000 °C, samples were constituted of a mixture of $UO_2$ and graphite, with some porosity deriving from the uncomplete packing of the powders and from reduction of $U_3O_8$ and $UO_3$ into $UO_2$. Fink [49] recommended a constant total emispherical emissivity of 0.85 for $UO_2$. Up to 1100 °C, the emissivity of the $UO_2C$ and $U_3O_8C$ samples was constant at 0.80 ± 0.02, while it increased for the $UO_3C$ sample from 0.76 ± 0.01 to 0.78 ± 0.01. For $T > 1100$ °C, emissivity increased for the three samples, and this corresponds to the beginning of carburization, as can be observed in Figs. 2 and 5. After sinterization, the emissivity of $UO_2C$ and $UO_3C$ was 0.86 ± 0.02, while for $U_3O_8C$ emissivity was 0.87 ± 0.01 at $T = 1600$ °C, in good agreement with previous unpublished results [50] that reports a similar value for porous $UC_2 + 2C$ samples. However, the previously measured emissivity data [46–48] report values much lower than 0.85 for uranium carbide (around 0.5). These differences can be attributed to different reasons:

(1) A compositional effect deriving from the amount of excess carbon within the samples; indeed, the uranium carbide prepared in this work is constituted of $UC_2$, C, a minor amount of UC and a non quantified amount of oxygen, while the uranium carbide analyzed by De Coninck [46] is nearly stochiometric $UC_2$ with a 99.5% theoretical density and 240 ppm of oxygen.
(2) A morphological effect deriving from the porosity present within the samples, as noted before (Table 2); the increase of emissivity with increasing the amount of porosity was previously reported in [51].
(3) A surface effect deriving from the observation that in the work of De Coninck the analyzed samples were polished before measurement, and this affects emissivity values as reported by many authors and also by this research group in [24].

## 4. Conclusions

$UC_x$ dispersed in graphite was successfully synthesized by carbothermic reduction of different uranium oxides ($UO_2$, $U_3O_8$ and $UO_3$) and excess graphite. Mass spectrometry studies revealed that the precursor oxides $U_3O_8$ and $UO_3$ decomposed to $UO_2$ before the carbothermic reaction started to occur, mainly with $CO_2$ emission, in good agreement with the literature. Further reduction of $UO_2$ may occur before carburization, so that the oxide that eventually reacted with graphite was hypo-stochiometric.

The carbothermic reduction started at $T > 1000$ °C, with CO evolution. The reaction was complete at 1600 °C, as confirmed by the comparison between calculated and measured mass losses. XRD analysis revealed the formation of a mixture consisting of α-$UC_2$, UC and graphite, confirming that the process is kinetically controlled.

From a morphological point of view, the $UC_x$ dispersed in graphite obtained from different uranium oxide precursors did not present significant variations in terms of grains size and porosity, indicating that the role of the uranium oxide precursor on the resulting carbide is not relevant. The total porosity ranged from 62.5 ± 1% to 64.4 ± 1.9% for all the samples, and only a small amount of it was closed porosity, which is advantageous for the specific application considered for these materials. SEM analyses showed the presence of macropores with a dual size distribution: pores of large dimensions (>10 μm), deriving from the carbothermic reduction reaction, and pores of few microns deriving from uncompleted sinterization of the carbide grains.

The reactivity of the $UC_x$ based composite in graphite vs. ambient air was investigated through SEM–EDS analyses. After 48 h of moist air exposure, the compositional changes of the sample surface as related to oxygen and carbon were evidenced through EDS spectra, but a precise determination of hydrolysis extent was prevented owing to the high experimental error on EDS compositional analyses. A deeper investigation on the hydrolysis rate of the composites is currently under development.

The measured emissivity for the three samples after sinterization at 1600 °C revealed a similar value for $UO_2C$, $UO_3C$ and $U_3O_8C$ samples, ranging from 0.85 to 0.88. The effect of porosity and composition of uranium carbide on the emissivity of materials is currently under study. The presence of unreacted uranium oxide within the sample was excluded by XRD analysis.

The produced $UC_x$ samples revealed a good fitting in terms of properties (density, open porosity and emissivity) with the SPES target requirements. Further studies are currently under investigation in order to tailor properties such as specific surface area and interconnectivity degree of the pores. The tailoring of the above mentioned properties should favor the effusion of the produced isotopic species and consequently the release efficiency of the target.

## Acknowledgments

Authors wish to thank the technical staff of LNL-INFN, M. Lollo, M. Giacchini and L. Costa for their precious support. Moreover, authors are grateful to Dr. G. Pavarin, responsible of the radiation protection service at the University of Padova, for his kind assistance.

## References

[1] H. Ravn et al., Nucl. Instrum. Methods B 26 (1987) 183.
[2] A. Kronenberg, E.H. Spejewski, B. Mervin, et al., Nucl. Instrum. Methods Phys. Res. B 266 (2008) 4267.
[3] Y. Zhang, G.D. Alton, Nucl. Instrum. Methods A 521 (2004) 72.
[4] C. Lau et al., Nucl. Instrum. Methods B 204 (2003) 246.
[5] A. Andrighetto, L. Biasetto, M. Manzolaro, et al., Applications of accelerators in research and industry AIP 1099 (2009) 728.
[6] A. Andrighetto, S. Cevolani, C. Petrovich, M. Santana, Eur. Phys. J. A 30 (2006) 591.
[7] A. Andrighetto, C. Antonucci, M. Barbui, S. Carturan, F. Cervellera, S. Cevolani, M. Cinausero, P. Colombo, A. Dainelli, P. Di Bernardo, F. Gramegna, G. Maggioni, G. Meneghetti, G.C. Petrovich, L. Piga, G. Prete, V. Rizzi, M. Tonezzer, D. Zafiropoulos, P. Zanonato, Eur. Phys. J. Spec. Top. 150 (2007) 273.

[8] R. Rundle, N.C. Baenziger, A.S. Wilson, R.A. McDonald, J. Am. Chem. Soc. 70 (1948) 99.
[9] L.M. Litz, A.B. Garrett, F.C. Croxton, J. Am. Chem. Soc. 70 (1948) 1718.
[10] R. Benz, C.G. Hoffman, G.N. Rupert, High Temp. Sci. 1 (1969) 342.
[11] C.A. Utton, F. De Bruycker, K. Boboridis, R. Jardin, H. Noel, C. Guéneau, D. Manara, J. Nucl. Mater. 385 (2009) 443.
[12] J.L. Henry, R. Blickensderfer, J. Am. Ceram. Soc. 52 (1969) 534.
[13] K. Maruya, J. Nucl. Sci. Technol. 7 (1970) 13.
[14] J.L. Henry, R. Blickensderfer, D. Paulson, J. Am. Ceram. Soc. 53 (1970) 335.
[15] J.M. Leitnaker, T.G. Godfrey, J. Chem. Eng. Data 11 (1960) 392.
[16] R.B. Holden, Ceramic Fuel Elements, an AEC Monograph, Gordon and Breach Science Publisher, New York, 1966.
[17] L. Biasetto, P. Zanoanto, S. Carturan, P. Di Bernardo, et al., J. Nucl. Mater. 378 (2008) 180.
[18] Y. Kawai, G.D. Alton, J.C. Bilheux, Nucl. Instrum Methods B 241 (2005) 991.
[19] L. Biasetto, S. Carturan, G. Maggioni, P. Zanonato, et al., J. Nucl. Mater. 385 (2009) 582.
[20] S. Carturan, M. Tonezzer, L. Piga, P. Zanonato, P. Colombo, A. Andrighetto, L. Biasetto, P. Di Bernardo, G. Maggioni, F. Gramegna, G. Prete, Nucl. Instrum. Methods Phys. Res. A 583 (2007) 256.
[21] P. Bricault, M. Dombsky, J. Lassen and F. Ames, Triumf Internal PrePrint, TRI-PP-07-31, November 2007.
[22] A Technology Roadmap for Generation IV Nuclear Energy Systems, DOE Report GIF-002-00, December 2002.
[23] G.C. Allen, J.A. Crofts, M.T. Curtis, P.M. Tucker, D. Chadwick, P.J. Hampson, J. Chem. Soc., Dalton Trans. (1974) 1296.
[24] L. Biasetto, M. Manzolaro, A. Andrighetto, Eur. Phys. J. A 38 (2008) 167.
[25] D. Manara, R. Pfliger, S. Sheindlin, Int. J. Thermophys. 26 (2005) 1193.
[26] C. Guéneau, M. Baichi, D. Labroche, C. Chatillon, B. Sundman, J. Nucl. Mater. 304 (2002) 161.
[27] P.-Y. Chevalier, E. Fisher, B. Cheynet, J. Nucl. Mater. 303 (2002) 1.
[28] T.B. Lindemer, M.D. Allen, J.M. Leitnaker, J. Am. Ceram. Soc. 52 (1969) 233.
[29] J.J. Katz, E. Raibinowitch, The Chemistry of Uranium Part 1. Element, Its Binary and Related Compounds, McGraw-Hill, New York, 1951.
[30] F. Poncet, F. Valdivieso, R. Gibert, M. Pijolat, Mater. Chem. Phys. 58 (1998) 55.
[31] S. Gossé, C. Guéneau, T. Alpettaz, S. Chatain, C. Chatillon, F. Le Guyadec, Nucl. Eng. Des. 238 (2008) 2866.
[32] S. Gossè, C. Guéneau, C. Chatillon, S. Chatain, J. Nucl. Mater. 352 (2006) 13.
[33] C. Guéneau, S. Chatain, S. Gossè, C. Rado, O. Rapaud, J. Lechelle, J.C. Dumas, C. Chatillon, J. Nucl. Mater. 344 (2005) 191.
[34] S.K.J. Mukerjee, J. Nucl. Mater. 199 (1993) 247.
[35] F. Poncet, F. Valdivieso, M. Pijolat, J. Nucl. Mater. 256 (1998) 155.
[36] L.M. Litz, A.B. Garrett, F.C. Croxton, J. Am. Chem. Soc. 70 (1948) 1718.
[37] S.K. Mukerjee, J. Nucl. Mater. 172 (1990) 37.
[38] E.K. Storms, Refract. Carbide. 171–213 (1967) 213.
[39] P.-Y. Chevalier, E. Fischer, J. Nucl. Mater. 288 (2001) 100.
[40] H.J. Emeléus, A.G. Sharp, Advances in Chemistry and Radiochemistry, vol. 12, Academic Press, NY, 1980.
[41] D.P. Stinton, S.M. Tiegs, W.J. Lackey, T.B. Lindemer, J. Am. Ceram. Soc. 62 (1979) 596.
[42] S.K. Mukerjee, J. Nucl. Mater. 210 (1994) 107.
[43] Y. Suzuki, Y. Arai, T. Sasayama, H. Watanabe, J. Nucl. Sci. Technol. 19 (1982) 222.
[44] J. Mildred, J. Bradeley, L.M. Ferris, Inorg. Chem. 3 (1964) 189.
[45] G.B. Engle, W.V. Goeddel, C.S. Luby, J. Am. Ceram. Soc. 45 (1962) 136.
[46] R. De Coninck, R. De Batist, A. Gijs, High Temp. High. Press. 8 (1976) 167.
[47] R. De Coninck, W. Van Lierde, A. Gijs, J. Nucl. Mater. 57 (1975) 69.
[48] M. Bober, H.U. Karow, K. Muller, High Temp. High. Press. 12 (1980) 161.
[49] J.K. Fink, J. Nucl. Mater. 279 (2000) 1.
[50] J.A. Nolen, M. Petra, J. Green, unpublished results.
[51] C.G. Progelhof, J.L. Throne, J. Am. Ceram. Soc. 52 (1969) 227.